Heat Transfer Modelling in Gas Turbine Stage

F. Martelli, P. Adami and E. Belardini
Energetic Dept. "S. Stecco"
University of Florence
via S. Marta, 3 Florence 50139
Italy

ABSTRACT

Two 3D CFD solvers for internal flow applications are briefly presented and applied for the investigation of heat transfer problems in gas turbine components. The numerical approaches considered are respectively based on a structured (XFLOS) and on an unstructured (HybFlow) methods. The two solvers are briefly described in terms of discretization scheme and turbulence modelling features for gas-turbine applications. Information are also provided concerning the unsteady approach, the multi-blok extension and the parallel porting of the two codes. These implementations are considered for improving the computational efficiency in the application to complex 3D stage investigations.

Particular care is demanded to the turbulent flow modelling which assumes great concern for heat transfer predictions on high loaded transonic turbine blades. According this observation, the two CFD approaches are initially applied to the heat transfer investigation of a 2D transonic turbine inlet NGV. Following this first assessment the thermal investigation of blade rows in considered for a 2D unsteady stage environment while further developments are finally reported for the 3D case.

1. INTRODUCTION

The computational fluid dynamics has become an effective tool for analysing complex flows and helping the design of more efficient turbo-machinery components. The advantage of the numerical approach lays in the chance offered for investigating many different working conditions from which global or detailed information about the flow can be extracted. In fact, the investigation of local effects of a machine component (cooling ducts, clearance passages, disk leakages…) and the analysis of detailed or unsteady flow quantities can be too expensive or complex for an experimental study under realistic conditions. This is especially the case for heat transfer predictions of transonic turbine stages. These applications represent a challenging and demanding request for a CFD numerical procedure since complex 3D steady and unsteady flow patterns develop, while shocks or wake systems interact strongly with wall boundary-layers greatly affecting the heat transfer load to the blade.

To this aim great importance has to be paid to the level of complexity of the mathematical model used and to approximation degree introduced to represent all physical mechanism active in the turbulent unsteady flow field of stage interacting rows. The mass averaged unsteady Navier-Stokes system of governing equations with a turbulence closure provided by the conventional eddy viscosity models are here considered. Concerning the stage flow field the basic procedure considered consist of the full unsteady coupling between the rows.

Both numerical efficiency and accuracy features are highly needed from the code for a realistic simulation. In this regard many applications of structured codes for 3D turbine investigations have been reported in literature using implicit ADI factorisation or multi-grid techniques.

A more sensible approach would instead refine the mesh locally only in region where a sharp variation of the solution is effectively expected. In this regard the use of the unstructured approach represent a promising strategy for heat transfer computations since it allows the needed high grid resolution close the solid boundaries with a reduced impact for the overall grid dimensions. Recently viscous unstructured code applications where reported for turbine stages by Kwon and Hah, 1995 and Mavriplis, 1995. Probably the first application of a 3D unstructured adaptive solution methodology in the turbomachinery area is represented by the work of Dawes, 1992 and an increasing effort has been addressed since then to the use of similar "geometrically flexible" approaches for internal flows. In fact, the main reason for this interest lays not only in the more rational mesh refinement allowed, but also in the higher geometrical flexibility allowing complex configurations to be represented and easily handled by the solution algorithm. In this regard most of known works actually do not fully take advantage of the great flexibility offered by the unstructured meshing and only recently the concept of grid transparency and hybrid mesh generation has been considered for practical computations (Connel and Braaten, 1995, Delanaye and Essers, 1997, and Haselbacher *et al.* 1999).

The aim of the present work is to apply and compare two solvers having a different concept (structured and unstructured) for internal viscous flows heat transfer investigation. Several turbulence closures are considered from the

Paper presented at the RTO AVT Symposium on "Advanced Flow Management: Part B – Heat Transfer and Cooling in Propulsion and Power Systems", held in Loen, Norway, 7-11 May 2001, and published in RTO-MP-069(I).

Report Documentation Page

Form Approved
OMB No. 0704-0188

1. REPORT DATE	2. REPORT TYPE	3. DATES COVERED
00 MAR 2003	**N/A**	**-**

4. TITLE AND SUBTITLE	5a. CONTRACT NUMBER
Heat Transfer Modelling in Gas Turbine Stage	5b. GRANT NUMBER
	5c. PROGRAM ELEMENT NUMBER
6. AUTHOR(S)	5d. PROJECT NUMBER
	5e. TASK NUMBER
	5f. WORK UNIT NUMBER
7. PERFORMING ORGANIZATION NAME(S) AND ADDRESS(ES) **NATO Research and Technology Organisation BP 25, 7 Rue Ancelle, F-92201 Neuilly-Sue-Seine Cedex, France**	8. PERFORMING ORGANIZATION REPORT NUMBER
9. SPONSORING/MONITORING AGENCY NAME(S) AND ADDRESS(ES)	10. SPONSOR/MONITOR'S ACRONYM(S)
	11. SPONSOR/MONITOR'S REPORT NUMBER(S)

12. DISTRIBUTION/AVAILABILITY STATEMENT
Approved for public release, distribution unlimited

13. SUPPLEMENTARY NOTES
Also see ADM001490, presented at RTO Applied Vehicle Technology Panel (AVT)Symposium held in Leon, Norway on 7-11 May 2001, The original document contains color images.

14. ABSTRACT

15. SUBJECT TERMS

16. SECURITY CLASSIFICATION OF:			17. LIMITATION OF ABSTRACT	18. NUMBER OF PAGES	19a. NAME OF RESPONSIBLE PERSON
a. REPORT **unclassified**	b. ABSTRACT **unclassified**	c. THIS PAGE **unclassified**	**UU**	**18**	

family of the two equation eddy viscosity models. Particular attention has been focused on models improvements concerning the physical realisability as well as extensions for the turbulence transition prediction.

Further, the application of the two approaches is discussed for future investigation of heat transfer in turbine stages. A 2D unsteady approach is applied and discussed for the stage problem analysis using the structured solver. The unstructured solver developments and preliminary results are described for the unsteady simulation of a 3D stator/rotor interaction.

2. MATHEMATICAL AND NUMERICAL MODEL

2.1 The governing equations for turbulent flows

The gasdynamic model considered is based on the classical Navier-Stokes systems of governing equations. In order to simulate high Reynolds viscous conditions a RANS (Reynolds Averaged Navier-Stokes) approach is applied for turbulent industrial flows. A Favre mass averaging is performed on the whole system while the family of two-equation eddy-viscosity models (eg. *k-ω*) is considered for the closure of turbulent stresses in the averaged equations. The resulting set of governing equations considered for internal viscous flows can be cast in strong conservative form as follows:

$$\frac{\partial Q}{\partial t}+\frac{\partial F_i}{\partial x_i}=\frac{\partial F^{v}{}_i}{\partial x_i}+S\ ,\ F_i=\begin{Bmatrix}\rho u_i\\ \rho u_1u_i+p\delta_{1i}\\ \rho u_2u_i+p\delta_{2i}\\ \rho u_3u_i+p\delta_{3i}\\ \rho Eu_i+pu_i\\ \rho u_ik\\ \rho u_i\omega\end{Bmatrix},\qquad F^{v}{}_i=\begin{Bmatrix}0\\ \hat{\tau}_{1i}\\ \hat{\tau}_{2i}\\ \hat{\tau}_{3i}\\ \hat{\tau}_{ij}u_j-\hat{q}_i\\ (\mu+\mu_T/\sigma_k)\dfrac{\partial k}{\partial x_i}\\ (\mu+\mu_T/\sigma_\omega)\dfrac{\partial \omega}{\partial x_i}\end{Bmatrix} \tag{1}$$

Here Q stands for the vector of the averaged variables, which characterise the flow field solution in terms of $\rho,\rho u_i,\rho E$ and the turbulent quantities $\rho k-\rho\omega$. All the governing equations within the flow field satisfy the same conservation balances obtained accounting for the accumulation, convection, diffusion, and production phenomena. The flux F_i represents the convective transport while $F^{v}{}_i$ is the diffusive counterpart. The tensor $\hat{\tau}_{ij}$ introduces the total turbulent-laminar stresses, while $\hat{q}_i$ accounts for the effective heat transferred by conduction. Thanks to the Boussinesq assumption the total stresses and heat conduction terms are expressed using the effective viscosity $\hat{\mu}=\mu_{lam}+\mu_T$ and the effective Fourier coefficient $\hat{\lambda}=\lambda_{lam}+c_p\mu_T/\mathrm{Pr}_T$ where Pr_T is a constant turbulent Prandtl number. The contribution to the source vector comes from the turbulence production and dissipation terms of the *k-ω* model. A source contribution appears also for the Navier-Stokes equation when a relative frame of reference is considered for the computation of the rotor row. In this regard the above equations are applied to model the rotor vane in a relative frame of reference, which is rotating with the blade itself. For ease of use, the same formalism has been retained for the fixed and for the rotating frame provided that when applied to the rotor row the velocity vector and all total quantities are assumed to be relative:

STATOR VANE	ROTOR VANE
$\vec{V}\rightarrow\vec{V}_{absolute}$	$\vec{V}\rightarrow\vec{V}_{rel}=\vec{V}-\vec{\Omega}\times\vec{R}$
$\rho E\rightarrow\rho E_{absolute}=\rho\left(e_i+\frac{1}{2}\vec{V}^2_{absolute}\right)$	$\rho E\rightarrow\rho E_{rel}=\rho\left(e_i+\frac{1}{2}\vec{V}^2_{rel}\right)$
$\Omega=0$	$\Omega\neq 0$

According the previous definitions the convective fluxes and the source terms *S* take the same expression regardless the stator or rotor row is considered:

$$S=\begin{Bmatrix}0\\ \vec{F}_{ce}+\vec{F}_{co}\\ \vec{F}_{ce}\cdot\vec{V}\\ P_k-\beta^*\rho\omega k\\ P_k\dfrac{\omega}{k}-\beta\rho\omega^2\end{Bmatrix},\quad \begin{matrix}\vec{F}_{ce}=-\rho\vec{\Omega}\times\left(\vec{\Omega}\times\vec{R}\right)\\ \vec{F}_{co}=-2\rho\left(\vec{\Omega}\times\vec{V}\right)\end{matrix},\quad S=\begin{Bmatrix}0\\ 0\\ \rho\Omega^2x_2+2\rho\Omega u_3\\ \rho\Omega^2x_3-2\rho\Omega u_2\\ \rho\Omega^2\left(x_2u_2+x_3u_3\right)\\ P_k-\beta^*\rho\omega k\\ P_k\dfrac{\omega}{k}-\beta\rho\omega^2\end{Bmatrix} \tag{2}$$

The perfect gas state equation is finally used to close the mathematical model: $p=(\gamma-1)\left(E-\rho\dfrac{\vec{V}^2}{2}\right)$

2.2 Transition Modelling

Two equation models represent traditionally a good compromise between accuracy and computational efficiency for prediction of turbulent flows. In order to verify the performances of two equation closures, several turbulence models of the two-equation eddy viscosity family have been implemented in both solvers and tested for a heat transfer prediction on transonic turbine blades. The accurate boundary layer definition assumes a relevant importance in heat transfer load simulation especially on the blade suction side where laminar/turbulent transition generally occurs in the adverse pressure gradient region before the trailing edge. The comparison of the heat transfer load on the blade against experiments allows therefore a valuable analysis of the turbulence closure performances for laminar/turbulent boundary layer computation. Except for the first algebraic approach, two equations models have been considered for such a purpose in the present work:

1) Baldwin-Lomax
2) *k-w* (low Re and High Re; Wilcox)
3) *k-e* (Launder-Sharma)
4) cubic *k-w* (Sofialidis-Prinos)
5) *k-g* (Kalitzin and Gould)

Despite the success of two-equation models for fully turbulent flows, several limitations arise when facing with the investigation of the transition problem. These can be summarised in a wrong location of the transition onset, under-prediction of transition length, too high sensitivity from initial conditions and weak dependency from the Mach number. In order to face transition modelling inaccuracies, the commonly used two-equations approaches are combined with integral methods or intermittency transport models. The integral methods attempt to characterise the boundary layer state by correlations based on the displacement or momentum thickness. Several correlations have been successfully proposed and tested in literature for turbomachinery applications such as the Abu-Ghannam and Shaw, 1980 and the Mayle, 1991. The Abu-Ghannam and Shaw correlation takes into account both the effect of turbulence level and pressure gradient. Conversely, focusing on turbulence levels above 3%, Mayle suggests a formula which accounts only for external turbulence intensity:

$$\mathrm{Re}_{\vartheta trans}=400\cdot Tu^{-5/8}$$

Integral methods determine the transition onset accurately and predict transition for attached flows, but require a considerable degree of empiricism for practical application to three-dimensional flows. In this regard all correlations require the turbulence level and velocity outside the boundary-layer, which is not clearly defined in complex 3D flows. These models still need an extra correlation for the intermittency function distribution downstream the transition onset. According the definition the intermittency γ assumes values between 0 and 1 from laminar to fully turbulent flow. The literature offers a wide choice of solutions such as that proposed by Simon and Stephens 1991:

$$\gamma=1-\exp\left(f\left(\mathrm{Re}_{\vartheta trans},s\right)\right)$$

being *s* the streamwise abscissa downstream the transition onset. An approach has also been suggested and tested by Michelassi and Rodi, 1997 using:

$$\gamma=\left(\frac{A_t^+}{A_t^+ + (300-A_t^+)\cdot\left(1-sin\frac{\pi}{2}\left(\frac{\mathrm{Re}_\theta-\mathrm{Re}_{tr}}{\mathrm{Re}_{tr}}\right)\right)}\right)^{\alpha}$$

The above expression suggests the shape of the function γ that reaches unity when $\mathrm{Re}_\theta=2\cdot\mathrm{Re}_{tr}$ and indicates also the transition length of the boundary layer downstream the onset point. The parameter α in equation controls the rise of γ in the transition region (the larger the value of α, the longer is the transition length). The eddy viscosity computed from the turbulence model is therefore expressed as follows:

$$\mu_t=\gamma\cdot C_\mu\cdot\frac{\rho k}{\omega}$$

The concept of intermittency function is based on the existence of a transitional boundary-layer, which is between a laminar and turbulent state. Despite experimental results indicate that transitional profiles are not a simple combination of laminar/turbulent solutions, the simplified assumption behind γ proves important success for practical applications (see Steelant and Dick, 1999). A simple application of the intermittency function approach can be defined coupling a two-equation closure to the intermittency function which is defined by the correlations defined above. A different approach suggested in literature is based on the evaluation of γ from its own transport equation which is solved throughout the computational domain. In this case the lack of history effects of zero equation correlation is overcome thanks not only to the kinetic energy and turbulent dissipation transport equations but also from the solution of the evolution equation for the intermittency function which is meant to improve the model physical basis. According the suggestion of Vicedo *et al.* the transport equation for γ is defined as follows:

$$\frac{D\gamma}{Dt} = \frac{\partial}{\partial x_i}\left[\left(\mu + \frac{\mu_t}{\sigma_\gamma}\right)\frac{\partial \gamma}{\partial x_i}\right] + \underbrace{c_{\gamma 1}\gamma(1-\gamma)\frac{c_\mu \rho k}{2R\varepsilon}P_k}_{\text{kinetic energy production}} + \underbrace{c_{\gamma 2}\rho\frac{k^2}{\varepsilon}\left(\frac{\partial \gamma}{\partial x_i}\right)^2}_{\text{self production}} \tag{3}$$

$$\underbrace{-c_{\gamma 3}\gamma\rho(1-\gamma)\frac{c_\mu \rho k}{R}}_{\text{dissipation}} \underbrace{-c_{\gamma 4}\gamma\rho(1-\gamma)\frac{k^2}{\varepsilon}\sqrt{k}\frac{U_j}{|U_k|}\frac{\partial U_i}{\partial U_j}\frac{\partial \gamma}{\partial x_i}}_{\text{entrainment}}$$

2.3 Structured Approach

The structured solver XFLOS is an implicit code based on the scalar form of the approximate factorisation method as proposed by Pulliam in order to reduce the computational costs of the implicit approximate factorisation method by Beam and Warming. The implicit matrix to be inverted comes out to be scalar penta-diagonal with a considerable savings of memory and CPU requirements for its inversion. Several variants of the basic scalar penta-diagonal solver are included ranging from the scalar tri-diagonal to the tri and penta diagonal block solvers using different versions of LU decompositions coupled with a diagonal dominance enhance (d3adi). The spatial discretisation is performed in the rectangular computational image of the physical domain by means of centred finite differences with second order accuracy in space. The artificial dissipation scheme is based on guidelines given by Jameson, 1981 and consists of a non-linear blend of implicit-explicit second order plus fourth order differences of the solution. A parallel version of XFLOS is also available under the MPI environment.

The implicit scalar approximate factorization is originally developed for the computation of steady flows. To take full advantage of the implicit formulation, the solver advances in time by using a local time step strategy. The unsteady time accurate solver introduces a double time step, as originally suggested by Jameson (1991) for explicit time marching algorithms, as shown in equation (1). The numerical time derivative (n) is used to advance in the numerical time with a local time step strategy. The physical time accurate derivative (p) acts like a source term, so that when the numerical time transient is eliminated, and the numerical time derivative is zero, equation (1) becomes an unsteady time accurate equation. Equation (1) is solved by the usual scalar approximate factorization in which the unsteady terms are treated implicitly as source terms. For further details about the algorithm see Michelassi et al. (1996).

$$\underbrace{\left.\frac{\partial Q_l}{\partial \tau}\right|_n}_{Numerical} + \underbrace{\left.\frac{\partial Q_l}{\partial t}\right|_p}_{Physical} + \left[\frac{\partial F_i}{\partial x_i} - \frac{\partial F_i^v}{\partial x_i} - S_l\right] = 0 \tag{4}$$

2.4 Unstructured Approach

The solver HybFlow performs a numerical discretization for the spatial gradients of the governing equation (1) using a cell centred finite volume scheme. The spatial discretization scheme is grid transparent and does not require any specific information on the local cell topology or element type, allowing a method which is suitable for generic unstructured hybrid grids. The computational domain is subdivided into an arbitrary set of 3D elements selected among exahedra, prisms, pyramids and tetrahedra covering without overlapping the whole computational domain. The numerical fluxes are computed integrating the flux function in equation (1) over all cell faces dividing every element from its neighbours. To this aim a simple midpoint quadrature formula is considered. The inviscid fluxes approximation is based on a reconstruction evolution approach. With the reconstruction phase the solution stored on the cell centres is interpolated onto faces mid-point considering a linear law. The solution monotonicity is enforced thanks to a slope limiting of the gradients using the solpe limiter defined by Barth, 1991 (Adami, 1998). The reconstructed values are considered to interact assuming an analogy with the evolution of a 1D and the resulting convective fluxes on the face are computed from solution of the Riemann problem with the Roe approximated method (Roe, 1986 and Barth, 1991). The viscous terms of governing equations are numerically integrated using a centred scheme based on the same FVM approach. The viscous stresses are computed on every element face using centred differences of the solution stored in

neighbouring elements. As far as spatial discretization no difference arise between the flow equations and these of the turbulence model.

The steady-state marching approach is based on the implicit time relaxed Newton method. The matrix of the implicit method is computed numerically approximating the derivatives of the vector with respect to the solution by finite difference expressions. The resulting linear system is solved at each integration step by the iterative method GMRES (Saad, 1994). To obtain an efficient convergence of the linear solution a right preconditioning is coupled with the iterative method. The preconditioning matrix is computed performing an incomplete ILU(0) factorisation of the implicit matrix (Saad, 1994). In the iterative time-marching scheme the two transport equations of the turbulence model are solved in a decoupled fashion. Therefore three separated and consecutively iteration steps are performed to march in time both the Navier-Stokes equations and the turbulent ones. In the first passage the 5x5 coupled system for mass, momentum and energy is considered and following two uncoupled implicit iterations are performed respectively for the turbulent kinetic energy and its specific dissipation rate.

The explicit time accurate discretization

Once the residual and source vectors in equation (3) are completely defined, the solution is advanced in time using a time accurate approach. In the present case an explicit time accurate multi-stage Runge-Kutta scheme has been considered. The general form of the method is:

$$Q_l^{(0)} = Q_l^n$$

$$Q_l^{(k)} = Q_l^n - \alpha_k \frac{\Delta t}{V_l}\left[R_l\left(Q^{(k-1)}\right) - S_l\left(Q^{(k-1)}\right)\right] \qquad k = 1, nk$$

$$Q_l^{n+1} = Q_l^{(nk)}$$

The model constants have been adopted according to a five step (*nk=5*) fourth order accurate multi-stage scheme in order to ensure good stability and damping properties: $\alpha_k = [1/15,\ 7/45,\ 2/7,\ 1/2,\ 1]$.

The implicit dual-time stepping discretization

With the dual-time stepping approach a numerical time derivative is added to the physical unsteady equations (1) producing the following expression:

$$\frac{\partial Q_l}{\partial \tau} + \left[\frac{\partial Q_l}{\partial t} + \frac{\partial F_i}{\partial x_i} + \frac{\partial F_i^v}{\partial x_i} - S_l\right] = \frac{\partial Q_l}{\partial \tau} + \left[\frac{\partial Q_l}{\partial t} + R_l(Q) - S_l(Q)\right] = 0 \tag{5}$$

Defining the unsteady residuals as:

$$R_l^*(Q) = -\left[\frac{\Delta Q_l}{\Delta t} + R_l(Q) - S_l(Q)\right]$$

then the governing equations assume the same form of a steady state problem

$$\frac{\partial Q_l}{\partial \tau} = R_l^*(Q_l)$$

The physical time derivative can be expressed using a second order back-ward finite difference:

$$\frac{\Delta Q_l^{n+1}}{\Delta t} = \frac{3Q_l^{n+1} - 4Q_l^n + Q_l^{n-1}}{2\Delta t} \tag{6}$$

A classical time marching approach is then recovered to drive to convergence the numerical unsteady term $\partial Q/\partial\tau$. Therefore, when a satisfying convergence criterion is achieved, then $R_l^*\left(Q^{(n+1)}\right) \approx 0$ and the physical unsteady solution at time level *n+1* is obtained. The time marching procedure is based on the approximate implicit Newton method for systems of non-linear equations obtained from a backward approximation of the pseudo time derivative of Q_l.

Replacing the physical time derivative with (6) and collecting together the terms of the implicit Jacobian matrix, the classical formalism of the implicit method is recovered:

$$\left\{\frac{I}{\Delta\tau} + J^*(Q^{(k)})\right\}\Delta Q_l^{(k+1)} = R_l^*\left(Q^{(k)}\right) \tag{7}$$

where

$$J\left(Q_l^k\right) = \frac{\partial}{\partial Q^{(k)}}\left[\frac{\Delta Q_l^{(k)}}{\Delta t} + R_l(Q^{(k)}) - S_l(Q^{(k)})\right]$$

2.5 The multi-block parallel extension (unstructured solver)

A common feature shared by all the applications considered for the unstructured solver is the high computational cost considering both CPU time and memory requirements. This aspect represents the main drawback of the code and can be considered a direct consequence of the implicit-unstructured architecture. In fact the most demanding phase of the solution algorithm lays in the implicit matrix storage and inversion required at every iteration step of the time marching procedure. These costs rapidly increase beyond modern computer capacities when complex or 3D viscous flows are considered. Therefore to improve the computational efficiency a multiblock procedure has been implemented into HybFlow with the primary objective of reducing the memory required by the solver. The multi-block strategy implemented in the code has a vertical mode structure and a complete iteration step of the time marching scheme is obtained processing sequentially every single block of the grid. Consequently the maximum dimension required for the storage of the implicit matrices is bounded to the dimension of the biggest block obtained from the mesh partitioning. Since each block is computed independently from the other then memory saving is achieved by the reduced dimensions needed by the linear solver GMRES during the implicit marching of each single grid-block.

The computing time also takes advantage from the decomposition of the entire computational domain into smaller blocks. In fact, while additional internal boundaries created among blocks lead to a reduction of the robustness of the solver (the consequence is an increase in the number of iterations), the overall CPU costs are reduced owing to the improving performances of GMRES for the implicit treatment of smaller grid portions.

Further, the domain decomposition method constitutes an essential step in view of the high computational demand expected for 3D unsteady simulations since it allows a straightforward implementation of the code on parallel architectures. The present parallel approach distributes individual portions of the overall grid among different CPUs. In this case all processors perform the same set of operations solving the flow field inside the sub-domains assigned to each CPU. Within the present strategy, providing almost the same number of elements inside each block, a uniform distribution of blocks to different PEs guarantees the required load balancing.

In figure 3a the flexibility of the of block decomposition strategy is underlined along with the communications paths needed to ensure the domain connectivity. The performances in terms of iterations count and CPU time are shown in Figure 2b. As observed the multi-block solver allows a reduction of the overall computing time using more blocks despite the increasing number of iterations required for the same residual reduction.

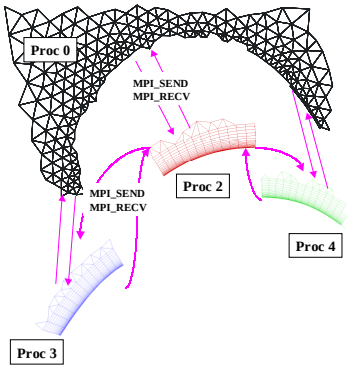

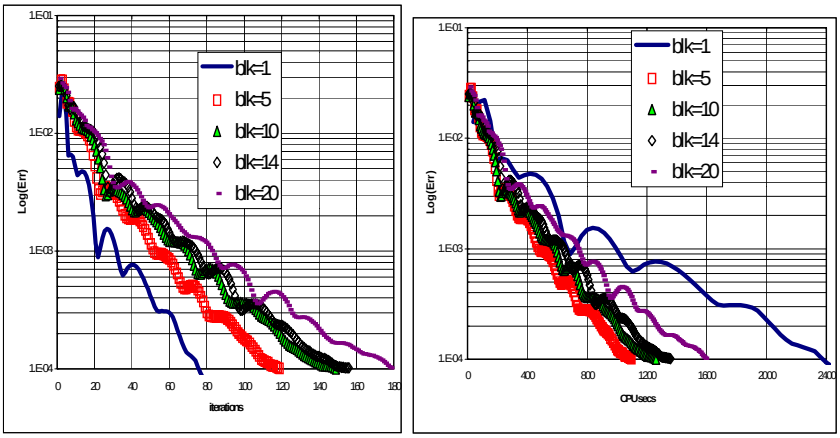

Fig. 1a: Parallel communications **Figure 1b: Residual History for the scalar/parallel solvers**

The parallel version of the code is based on the standard MPI message passing libraries to ensure high portability. The neighbouring elements residing on the local memory of different CPUs require the explicit activation of a communication procedure among processors to satisfy the physical flow continuity. Owing to the multi-block structure of both the implicit (eg. the spatial discretization, the implicit linear solver GMRES) small changes have been required for the porting of the code to parallel architectures.

3. TURBOMACHINES APPLICATIONS FOR HEAT TRANSFER

Two applications will be here discussed concerning internal flows of turbomachinery interest. In the first an investigation focused on the heat transfer prediction is reported concerning a 2D transonic NGV blade (VKI Ls89). Several turbulence models and transition approaches will be summarised underlining their ability and performances for the accurate prediction of the laminar-turbulent transition and heat transfer load. The second test case concerns the more detailed investigation of the basic CFD features in the simulation of a 3D transonic turbine stage. This application will provide useful information about the accuracy and capability of single blade CFD computations tools in the design and analysis of the stage components. The structured solver is applied using a stage mixing plane strategy for stator/rotor matching. The unstructured code assumes, for the stage analysis, the inter-stage conditions computed from a previous fully unsteady inviscid stator/rotor investigation. In this case the stage matching is ensured by the unsteady simulation

which can be performed at reasonable computing cost: the time averaged inter-stage conditions are then imposed at the NGV exit and rotor inlet plane. More details of the unsteady stage approach and investigation are reported by Belardini et al., 2000, Adami et al., 2000.

3.1 NGV Blade Heat Transfer

The following application considers the 2D blade LS89 investigated by Arts *et al*., 1990. The grid features and blade geometry are shown in the following Fig. 2. The blade chord is C=67.647 mm with a pitch/chord ratio of 0.85. The main characteristics of both the blade and the test conditions will be here reported, while for a more detailed description the work of Arts *et al*. 1990 should be considered. The structured I type grid (Fig. 2-b) consist of about 33000 nodes and has been used for the structured solver XFLOS. For the hybrid unstructured approach (Fig. 2-c), a structured O type region around the blade wall is coupled with an outer unstructured part covering the remaining flow domain (14500 mixed triangle/quadrangle elements) and the solver HybFlow has been considered.

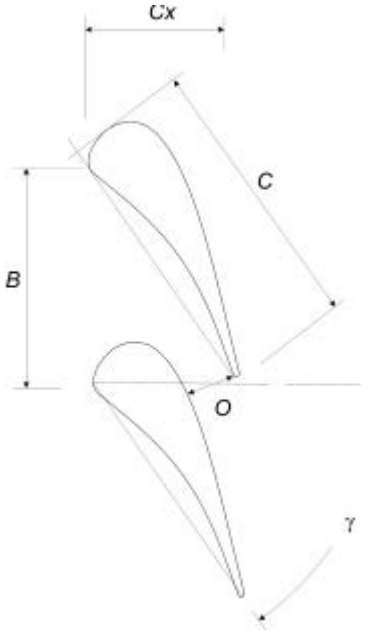

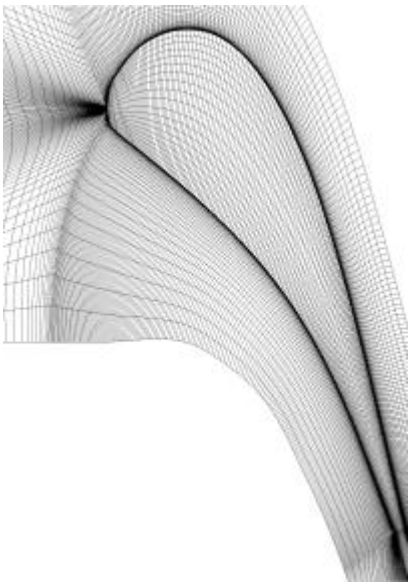

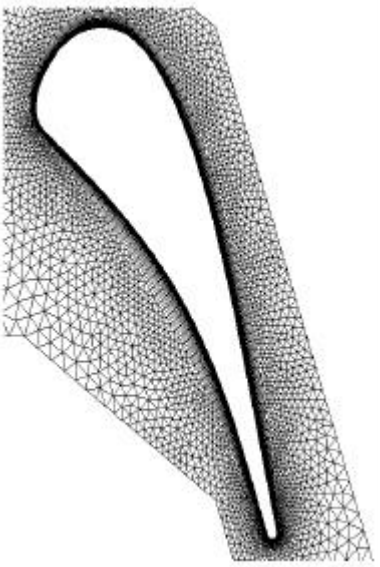

Figure 2a: Blade Geometry **Figure 2b: Structured grid** **Figure 2c: Unstructured grid**

Several Reynolds numbers and the outlet pressure conditions have been reported by Arts for a comprehensive aerodynamic and thermal investigation of the transonic flow. Computed pressure profiles are compared against experiments in Fig. 3, for a coarse grid unstructured computation based on 7000 elements (MUR43 corresponds to an outlet isentropic Mach of 0.84; MUR47 to a higher outlet value of 1.02).

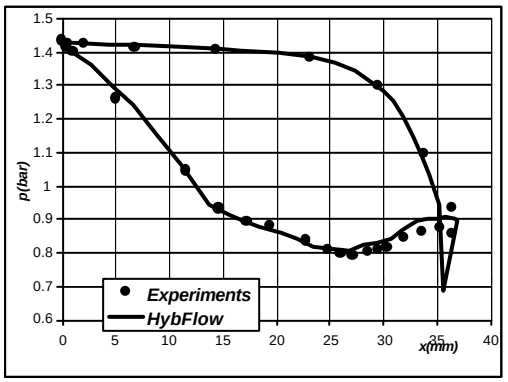

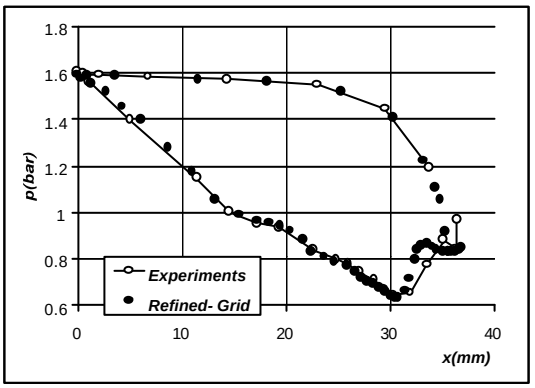

Figure 3a: test MUR43 **3b: test MUR47**

In figure 4 and 5a the heat transfer coefficient is reported for the blade surface comparing several computations among them and against experiments. The test conditions are referring to the Test MUR241: Re(out)=2E6, Mis(out)=1.09 and incoming turbulence level Tu=6%. As observed, despite the different structured/unstructured implementation, all turbulence closures presented shows the same tendency to anticipate transition on the suction side of the blade regardless of the inlet flow turbulence level and turbulence length scale. All the test performed show that traditional approaches basically fail and cannot reproduce transition. More detailed analysis show that the leading edge

treatment is not responsible for the inaccuracies which are independent of the adoption of ad-hoc corrections such as Kato-Launder or other realizability constraints.

Further the analysis shows that linear constitutive laws perform approximately like non-linear closures while the choice of transported variables appear not playing a crucial role (k-g or k-ε performs similar to k-ω). The implementation of the intermittency transport equation in the turbulent closure does not improve by itself the modelling performances (Figure 5a).

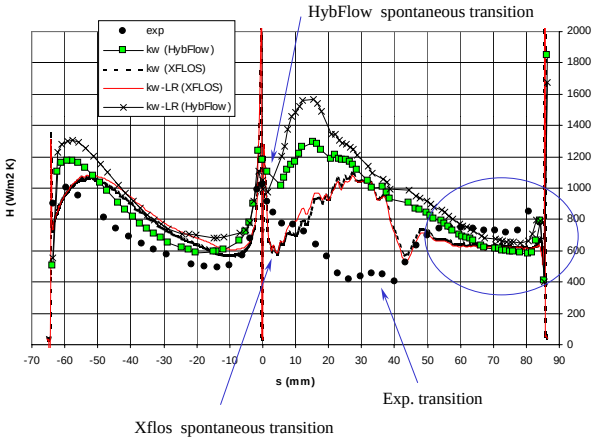

Figure 4a: structured/unstructured solvers

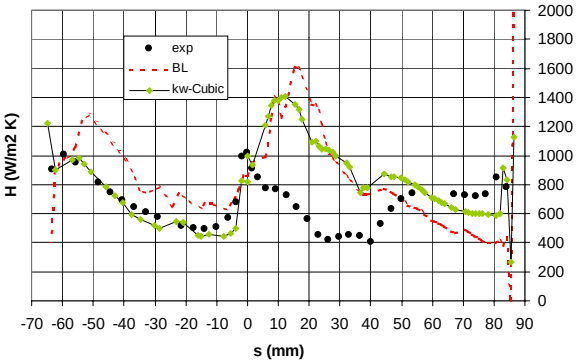

Figure 4b: non linear and algebraic closures

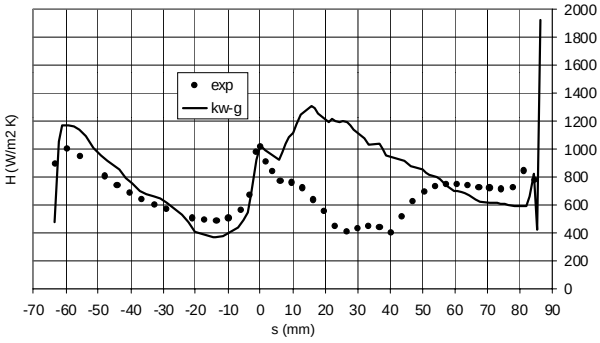

Figure 5a: *k-ω* with γ transport equation

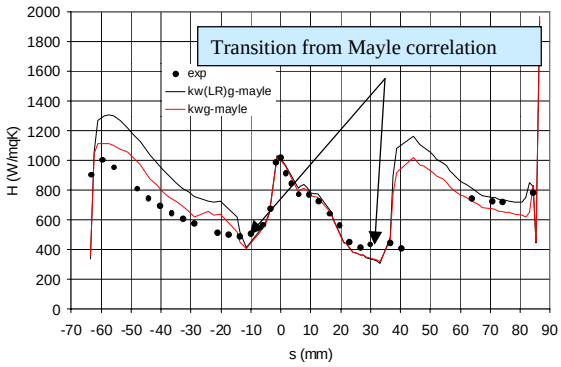

Figure 5b: Mayle transition onset

The transition modelling approach based on the integral Mayle correlation proves a remarkable success in predicting the onset of laminar turbulent transition. Nevertheless, as shown in figure 5b, 6a and 6b, the use of the Mayle correlation alone, although effective for the transition onset, does not guarantee a correct estimate of the transition length. A sudden transition is generally observed in all tests downstream the onset that is provided by the correlation and a miss-prediction of the heat transfer profile is appreciated especially on the blade suction side. This behaviour is evident regardless the addition in the two equation closure of the intermittency transport equation (3).

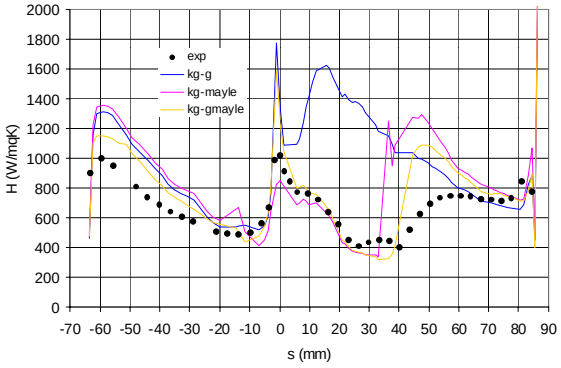

Figure 6a: *k-g* modelling

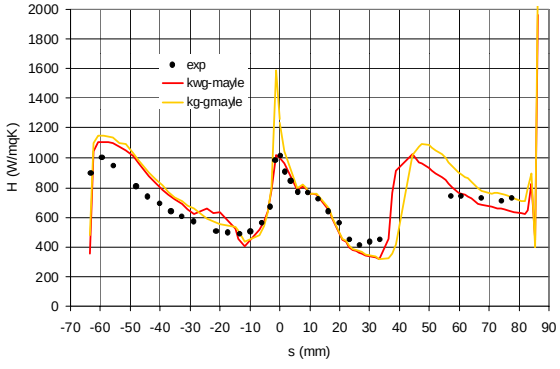

Figure 6b: *k-ω–γ* and *k-g-γ* models with Mayle

The use of a second correlation for the transition length has been therefore considered for the improvement of the computation accuracy downstream the onset. For easy of use the Rodi-Michelassi correlation has been applied with the basic two equation *k-ω* model and Mayle criterion. The heat transfer profile shown in Figure 7a proves an improved

agreement with experiments. Similar results come from the same use of the correlations approach using different two-equations turbulent closures.

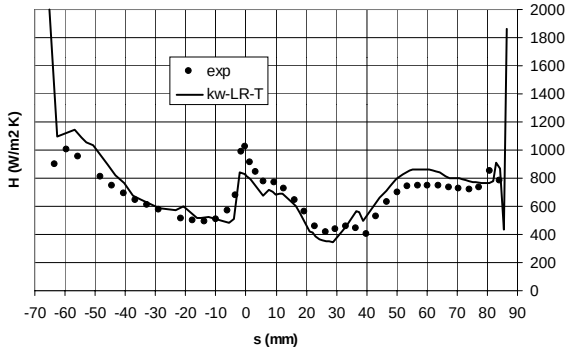

Figure 7a: test MUR43

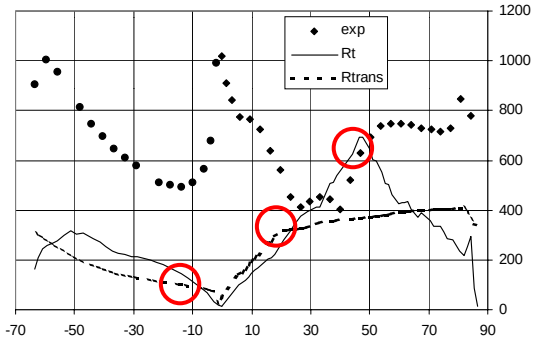

Figure 7b: test MUR47

The good agreement can be justified from the profiles of momentum thickness reported in figure 7b. As observed the computed Re_{ϑ} exceeds the transition value obtained from Mayle correlation at the expected abscissa on both suction side and pressure side of the blade. On suction side transition is completed from the Rodi-Michelassi correlation just before s=50 where the experimental heat transfer coefficient stabilises at the value for fully turbulent flow.

A different flow condition Test MUR116 has been considered: Re(out)=2E6, Mis(out)=1.09, Tu=0.8%. The heat transfer distribution is shown in Figure 8a for different model arrangements all using the transition onset from Mayle correlation. The agreement on pressure side is satisfactory especially considering the *k-ω* model. On the pressure side the Mayle correlation detects the correct onset for transition which occurs around s=80. Nevertheless, in the region between s=40÷75 ahead the transition, the computation underestimates appreciably the heat transfer growth observed in the experiments.

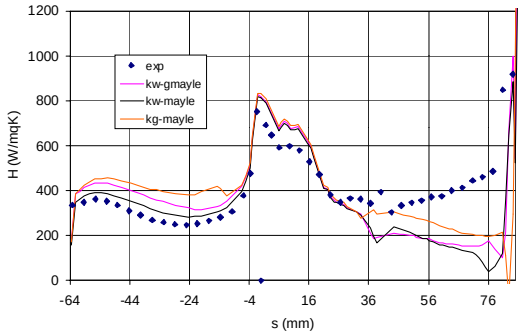

Figure 8a: test MUR43

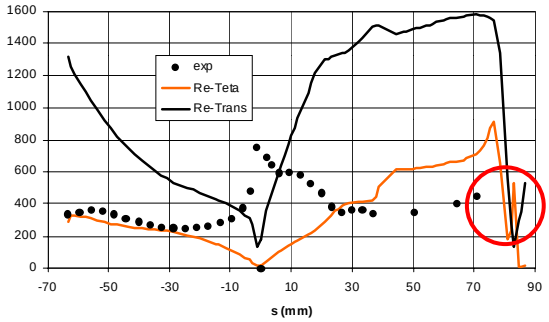

Figure 8b: test MUR47

3.2 2D Unsteady Stage Computations

Test Rig Description

The model has been applied to the analysis of the stator-rotor interaction in a transonic turbine with special attention to the unsteady aerodynamics and heat transfer, the crucial importance of which is becoming more and more evident. In order to apply the code to a realistic configuration for which a set of experimental data points were available, the HP turbine developed in the framework of the BRITE-EURAM programme was selected. Such a configuration includes the effect of the coolant ejection from the trailing edge of the stator blade. which required an additional modelling effort in the code described in the following section. A brief description of the cascade is here presented while for a detailed description of the experimental rig the work of Denos et al., 1999 should be considered. The BRITE turbine stage is composed of one stator and one rotor row. The first contains 43 untwisted cylindrical vanes while the rotor blade row consists of 64 twisted blades. The NGV blades also present a pressure side cut for trailing edge coolant ejection. The NGV/rotor blade count ratio is close to 2:3 (0.6718 against 0.6667) exact periodicity is obtained with a slightly modified pitch ratio using 2 vanes and 3 blades. The stage geometry is shown in Figure 9 and 10 along with the 3D inviscid grid used to perform stator/rotor interaction (about 350000 elements). At the NGV pressure side a cut in the blade is used for trailing edge coolant ejection. The coolant mass flow ejected at the blade cut is 3% the total NGV inlet mass flow rate. Wide measurement campaigns have been performed in different aero-thermodynamic conditions by Denos et al., 1999. The behaviour of the HP turbine stage at nominal, low and high pressure ratios has been investigated

in steady and unsteady environment. In the present work nominal unsteady flow field conditions will be accounted. (P_{01}/P_3 = 3.06): P01=1.62 [bar], T01=440 [K], Mis (exit NGV)=1.08, M(exit rotor)=0.42, W=10.9 [Kg/s].

Structured 2D Simulation

Although the experiments are carried out on a annular test rig, the computer simulations are run in a two dimensional midspan geometry to reduce the computational effort. The computer program, coded in 3D, is used here in a 2D manner by solving one control volume only in the radial direction. The stator and rotor blade rows are then assumed to be linear. The I-type grid, shown in figure 9 for inviscid computations. is one of the most general possibilities when staying with simply connected or single block grids. The grids are nearly orthogonal in the crucial stagnation point region.

The exact stator pitch at midspan is P_s =54.0427 mm, while for the rotor row the pitch is P_r=36.3099 mm. To have a nearly periodic problem one can solve two stator blades and three rotor blades since the pitchwise extension of the stator is $2\times P_s$=108.0854 and the pitchwise extension of the rotor is $3\times P_r$=108.9297. To have a fully periodic calculation the previous two lengths should be equal. Since the mass flow rate is controlled by the size of the stator row, it was decided to keep the dimensions of the stator row unaltered and change the dimensions of the rotor row to have $2\times P_s=3\times P_r$.

The experimental total pressure, temperature, and inlet flow angle are specified at the stator inlet. The rotor exit static pressure is given to match with the experimental conditions. The measured inlet turbulence level (1.6%) is fixed at the stator inlet section. The inlet turbulence length scale, selected on the basis of a previous validation of the model (Michelassi et al.[19]) against similar wind tunnel data, is $1\%P_s$. A viscous adiabatic condition is set on the stator blade surface, while the experimental surface temperature is fixed on the rotor blade, where the velocities are set to zero and the static pressure is computed by using a zero derivative normal to the wall. On solid walls the turbulent kinetic energy is set to zero and ω has a constant value on the solid boundaries (Wilcox[12]). On the subdomains interfaces the grid point distribution is not periodic and the solution is ensured to be continuos by extending the grid of each subdomain which overlaps on the neighboring sub-domain. Details of the grid overlapping can be found in Michelassi et al.

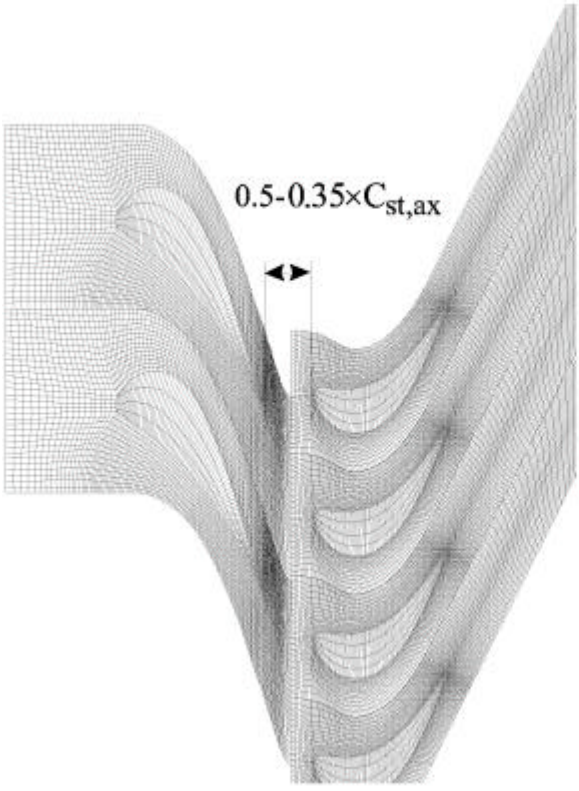

Figure 9. Grids for inviscid calculations (very coarse grid, stator 168×33 - rotor 173×33

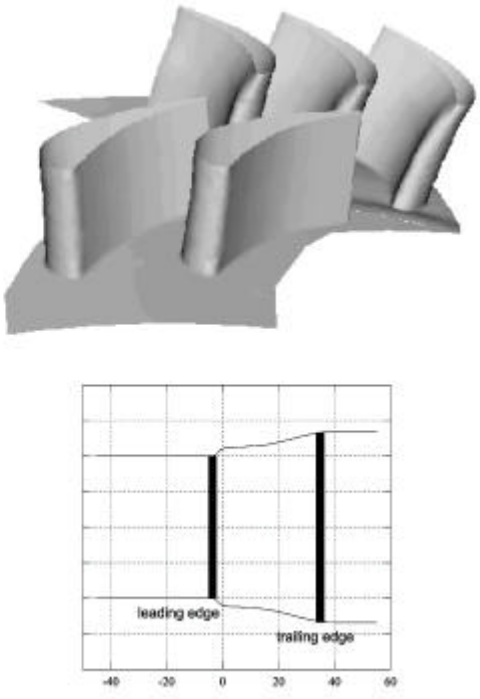

Figure 10. Qualitative shape of the rotor channel

The dimensions of the rotor row are changed by reshaping the pitch and the blade size by a scaling factor $SC=2\times P_s/3\times P_r$=0.992249. In this way the overall rotor row is reduced in size by a factor 0.775%. While the stator has a constant height, the rotor passage has the variable height in the test rig qualitatively sketched in figure 2. The small reduction in the rotor throat area was then compensated by the grid expansion in the radial direction. This shape of the channel requires a quasi-3D calculation which is simulated by using a variable cross section thickness in the radial direction. The spanwise expansion of the rotor channel was further adjusted so as to match the measured mass flow rate.

Transitional Flow Calculations - Large Gap (0.5×<Cax)

In this configuration the axial distance between the stator t.e. and the rotor l.e. is $0.5 \times C_{ax,s}$. The large gap case is computed without and with the stator pressure side coolant ejection and at the nominal 6500 RPM. The coolant mass flow rate is 3% of the overall mass flow rate.

Figure 11 compares the computed and measured average M_{is}. The profiles are averaged over a full rotor revolution for the experiments and over one passage of a rotor vane in front of two stators after a periodic-in-time solution is achieved for the computations. The coolant jet flow is evident in figure 11,b and c which shows the difference of vector profiles with and without coolant ejection.

The effect of the coolant jet on the rotor fades away, as proved by the M_{is} profiles in figure 11,1. There are only marginal differences in the averaged isentropic Mach number profiles, and these are due to the small changes in the wake depth caused by the coolant jet.

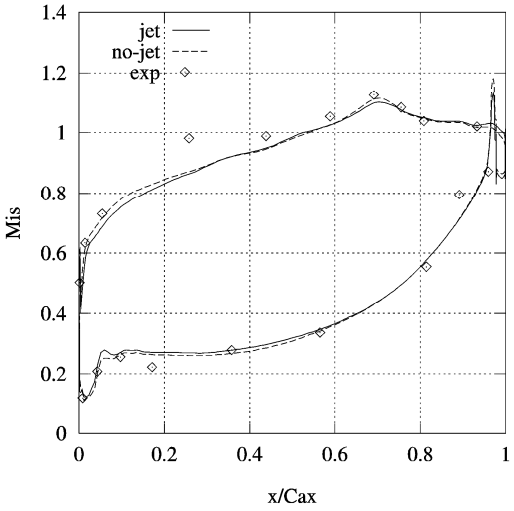

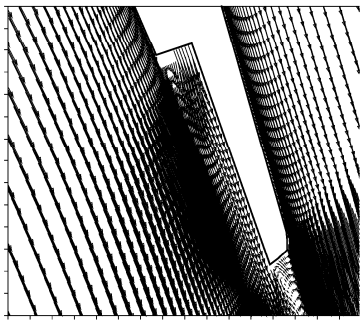

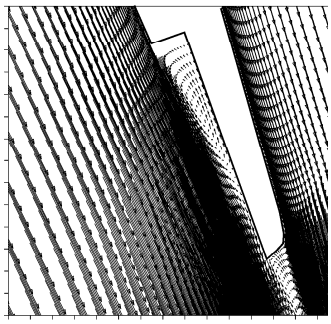

Figure 11a: Isentropic Mach Number profiles **(b) q_{jet}=0%** **(c) q_{jet}=3%**

The analysis of the heat transfer is made by comparing the measured and computed Nusselt number over the rotor surface. The leading edge is positioned at s=0 and the curvilinear wall distance is normalized by the distance of the last measured point on the suction side. Figure 14 compares the averaged Nusselt number in which the experiments have been conducted only with the cooling jet. The computations with the coolant jet are closer to the experiments on both the suction and the pressure sides, although in the leading edge region the code predicts values of Nu which are smaller than the experiments.

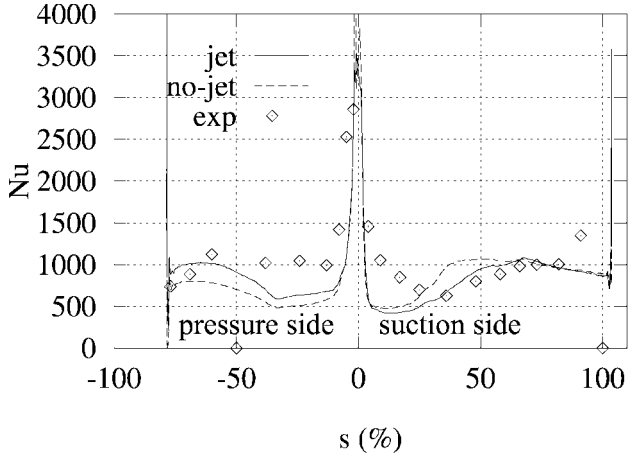

Figure 12. Nu profile with/without jet, large gap

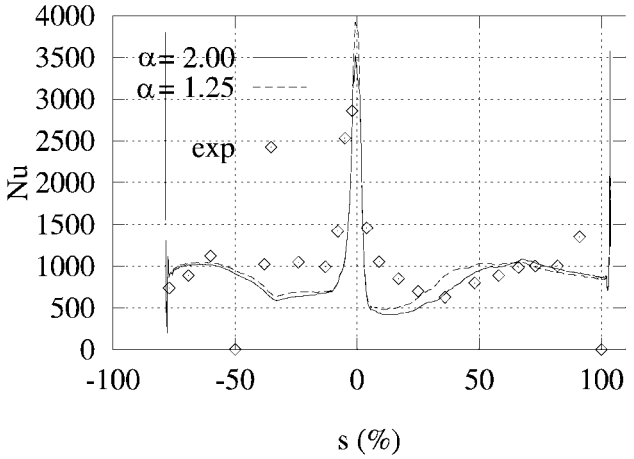

Figure 13. Effect of model modifications on Nu

The agreement rapidly improves when moving downstream. The small level of the predicted Nusselt number in the range -20%<s<20% is not likely to be caused by an insufficient turbulence level predicted in the leading edge region since the turbulence levels are well above 5 to 10%, which is more than enough to induce transition. The exponent α in equation for transition length correlation allows the extent of transition to be controlled. Values of α above unity and smaller than two induce a steep rise of the intermittency function thereby reducing the transition length. Moreover figure 13 indicates that when reducing α from 2.00 to 1.25 the situation marginally improves in the range -20<s<20.

Apparently, the underestimation of Nu close to the leading edge is partly governed by some inaccuracy in the aerodynamics prediction. This is proved by figure 14 in which the predicted averaged, minimum and maximum values of M_{is} are compared with the respective measurements.

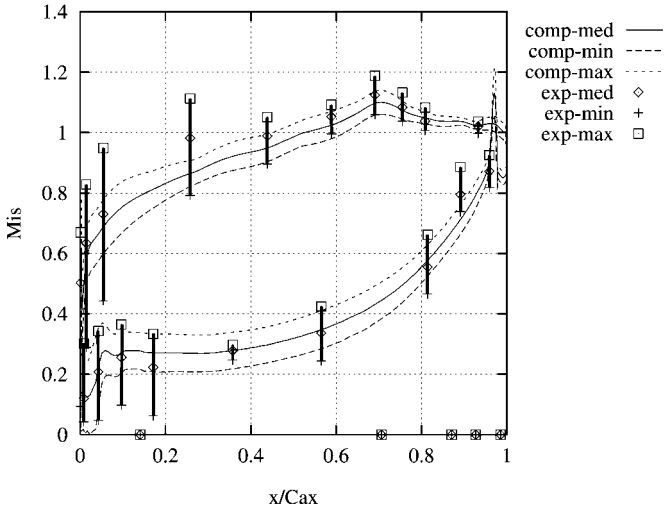

Figure 14. Isentropic Mach number fluctuation range

On the pressure side, and on the suction side for x/Cax>0.45, computations and experiments agree on both the average and the minimum and maximum values. The agreement deteriorates on the leading edge suction side where the code predicts velocity levels up to 20% smaller than what is indicated by the experiments. This disagreement is stemming from an underestimation of the angle of attack in some wake interference configurations. Moreover, as proposed by Giles, the shock departing from the suction side of the stator trailing edge impinges on the nose of the passing rotor blade thereby inducing large pressure fluctuations. The predicted pressure, and M_{is}, fluctuations are somewhat smeared because of the grid skewness which introduce some numerical diffusion.

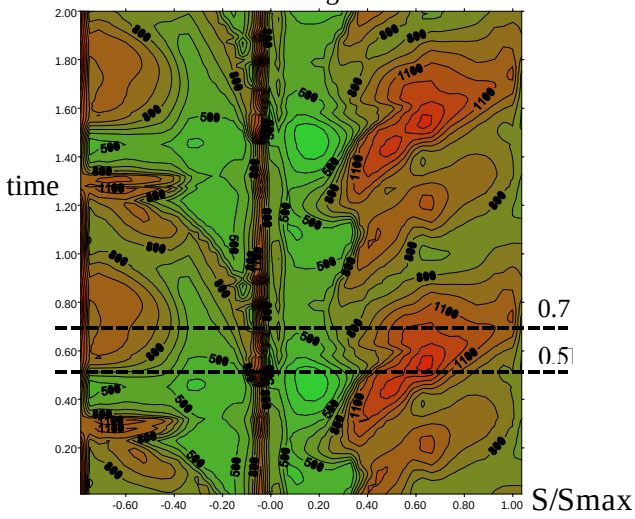

Figure 15a: Nu profiles q_{jet}=3%.

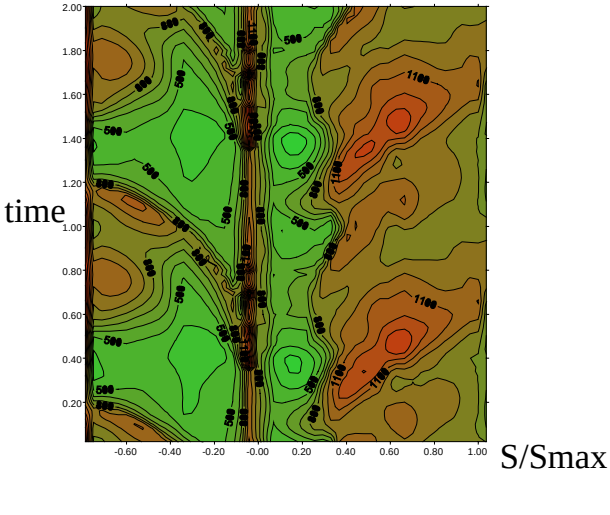

Figure 15b: Nu profiles q_{jet}=0%

The effect of the passing wakes on the rotor heat transfer can be traced in figure 15 which shows how the peak of Nu is moving downstream. It is now easy to follow the development of the transition point in time. The triggering effect of the wake is not very large since the transition point on the suction side ranges between 0.2<S/Smax<0.38 regardless of the presence of the cooling jet. This is understandable on account of the large turbulence level which is mainly responsible for the onset of transition, at least in the computer simulation code. The peak on Nu tends to smear in time and apparently the heat transfer increases in time while approaching the trailing edge because of the mentioned effect of the wake. This phenomenon is caused by the developing transition of the boundary layer. When comparing the steps 0.5 and 0.7 the isolines spread in space and the Nusselt number increases also in the upstream direction for both the q_{jet}=0% and 3% mass flow rate cases. In such a situation the computations indicate that the boundary layer thickness has increased and the elliptic flow region close to the rotor blade suction side has grown. This elliptic effect can have a large impact on the determination of the hot spots on the rotor blade.

Transitional Flow Calculations - Small Gap (0.35×<Cax)

When reducing the gap between the blade rows the overall flow pattern remains unchanged. Figure 16 shows the isentropic Mach number profiles on both the stator and rotor blades. The stator behaves very similarly to the larger gap case, while the rotor shows some differences with respect to the larger gap case especially in the throat. Apparently the average pressure distribution on the rotor feels the stronger disturbances coming from the stator row because of the shorter distance the wake and the shocks have to travel. Surprisingly, this has weak impact on the averaged heat transfer rate that shows very little changes with respect to the $0.5\times C_{ax}$ case (see figure 17).

The computations like the experiments do not show a clear average onset of transition on the suction side, unlike the $0.5\times C_{ax}$ case in which the onset of transition was clearly detectable at s/smax≈30. Experiments and computations agree in indicating a nearly flat Nusselt number distribution on the blade suction side. The pressure side profile is almost identical to the larger gap case with the same underestimation of the heat transfer rate which extends up to 50% of the blade. Overall, the $0.35\times C_{ax,s}$ gap case does not give any extra information with respect to the $0.50\times C_{ax,s}$ case in terms of unsteady behavior and flow angles, as also indicated by Michelassi et al.

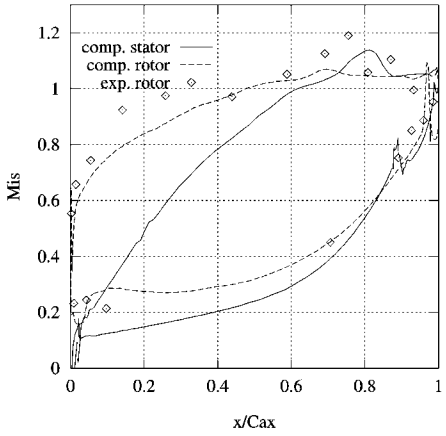

Figure 16: Isentropic Mach Number profiles.

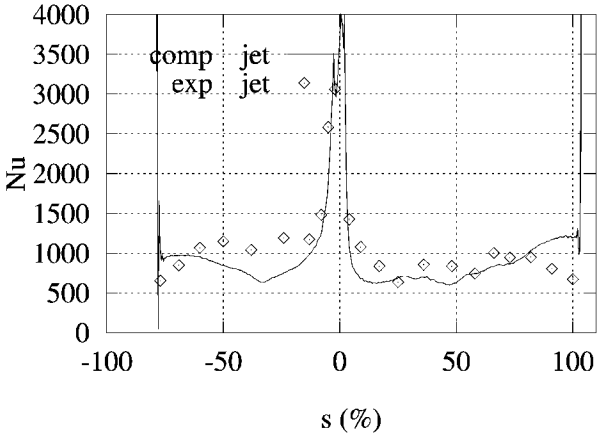

Figure 17: Nu profile with jet, small gap.

3.3 3D Unsteady Stage Computations

The computation for 3D heat transfer for unsteady working conditions on the rotor blade in under development using the unstructured solver. To this aim the code have been adapted to approach the full 3D stage environment with the unsteady time accurate algorithms described in 2.4. The preliminary validation of the computational procedure has been carried out following two different integration strategies based on the implicit dual time step approach or the explicit multi-step Runge-Kutta method. The high costs involved with such approach are faced using a parallel version of the solver as discussed in 2.5. The details of results obtained from the unsteady preliminary computations can be found in Belardini et al., 2001. The approach developed is based on the reduced count approach considering a blade ratio of 2:3 between the NGV and rotor rows. The coarse computational grid for unsteady stage computations is reported in figure below.

The approach proves to be effective for the computation of the aerodynamics characteristics of the full stage. As observed from figure 19 the time averaged interstage pressure profiles agree reasonably with experiments.

To reduce computational costs the features of the unstructured grid approach are highly exploited. A thin layer of prismatic elements is placed close solid boundaries for the accurate prediction of the boundary layer while full unstructured elements are placed in the vane passage and in the interstage between the two rows. The geometrical flexibility of the approach is considerably useful for adapting the mesh at the NGV trailing edge where coolant ejection is provided from the pressure side blade cut. The grid is further refined downstream in order to accurately reproduce the NGV wake which is impinging onto the rotor leading edge. The same features of the unstructured grid allow a local refinement at the rotor tip for the direct computation of the leakage flow.

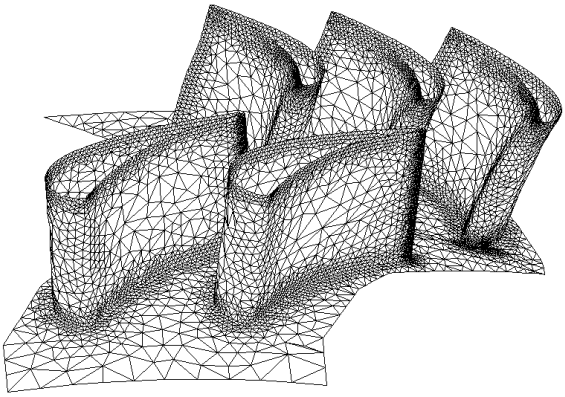

Figure 18: Stage coarse grid

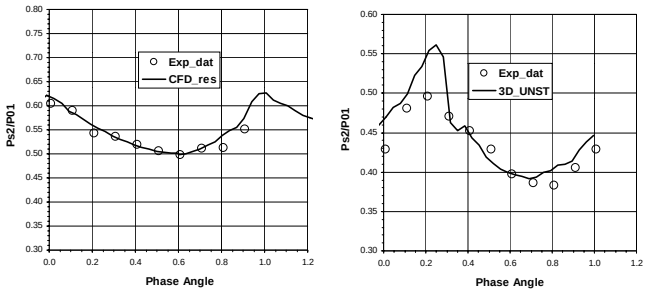

Figure 19: Hub and shroud wall pressure

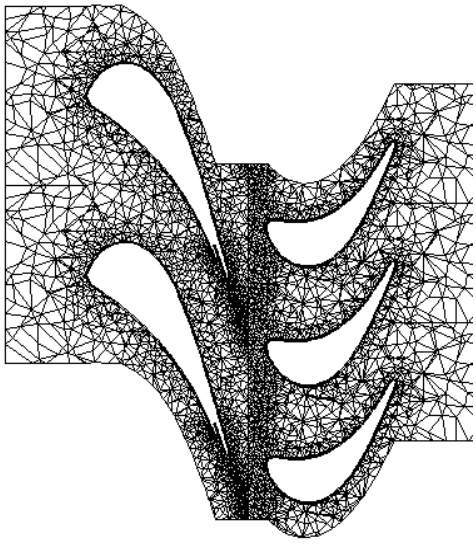

Figure 20a: mid-plane viscous

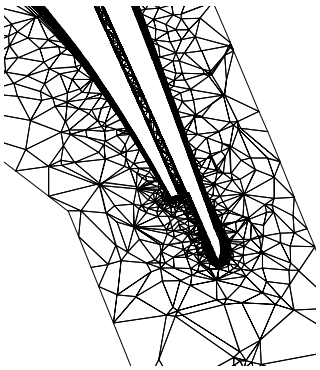

Figure 20b: NGV T.E.

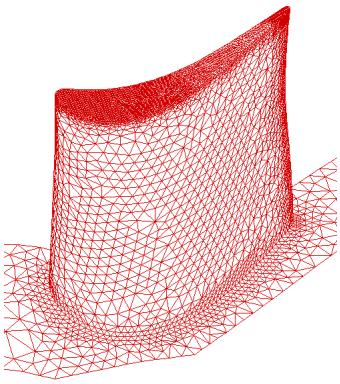

Figure 20c: rotor blade

The governing equations on the rotor row are solved on the relative frame of reference and a sliding mesh approach is used to mimic the rotational speed behind the NGV blades. The grid geometry in correspondence of the rotor stator boundary is fully three-dimensional and unstructured according to the grid generation requirements in the inter-stage gap. In order to guarantee a simple and robust matching law, the solution is exchanged between the two rows using a 2D interpolation scheme at the interfacing grid-plane.

4. CONCLUSIONS

The problem of heat transfer prediction has been considered for turbine applications considering two different numerical strategies. The differences of the schemes are highlighted considering the spatial discretisation and the time accurate integration scheme. Different turbulence modeling closures have also been discussed and compared, concerning heat transfer prediction, among them and between the two codes described for a 2D high loaded transonic turbine blade. The unsteady flow field in a 2D transonic turbine stage has been computed by the structured N-S solver. The results were compared with experiments in terms of blade load, rotor blade pressure and Nusselt number distribution. The computed results compare favorably with experiments. In particular the computation were found able to reproduced the rotor blade load fluctuations with a good degree of accuracy. In terms of heat transfer, the accuracy of the predictions deteriorated in proximity to the rotor leading edge, where the Nusselt number is underestimated. Still, the computations seem to capture the essential features of the flow not indicating a clear onset of transition. The computations proved that both the stator and rotor vanes are highly unsteady, and that large disturbances, in terms of static and total pressure, reach the rotor row in which the heat transfer rate exhibited a highly unsteady behavior, but, although the code is able to capture the essential features of the flow, more work is needed in the field of unsteady transition. The work in progress for the 3D approach to the problem is finally presented for the unstructured parallel solver, showing the capability of the method and the possibility offered to catch the more complex phenomena which exist in the real 3D configuration.

References

Abu-Ghannam, B.J., Shaw, R., "Natural Transition of Boundary Layers - The effects of Turbulence, Pressure Gradient, and Flow History", Journal of Mechanical Engineering Science, 1980, Vol.22, No.5, pp.213-228.

Adami P., Martelli F. and Michelassi V., 2000, "Three-Dimensional Investigations for Axial Turbines by an Implicit Unstructured Multi-block Flow Solver, AMSE, IGTI TurboExpo 2000, Munich.

Adami P., Michelassi, V., Martelli, F., 1998 "Performances of a Newton-Krylov scheme against implicit and multi-grid solvers for inviscid flows" AIAA paper 98-2429.

Adami, P., 1999 "Computations for internal flows with a low-mach preconditioned Newton-Krylov scheme", 3rd European Conference on Turbomachinery. London

Addison, J.S., Hodson, H.P., 1992, "Modelling of Unsteady Transitional Boundary Layers", ASME Journal of Turbomachinery, Vol.114, July, pp. 580-589.

Arts, T, Lambert de Rouvroit M. and Rutherford, A.W., 1990, "Aerothermal Investigation of a Highly Loaded Transonic Linear Turbine Guide Vane Cascade" VKI tech. Not. 174.

Barth, T.J.,1991 "Numerical Aspects of Computing Viscous High-Reynolds Number Flows on Unstructured Meshes", AIAA Paper 91-0721, Jan.

Beam, R.M., Warming, R.F., 1982, "Implicit Numerical Methods for the Compressible Navier-Stokes and Euler Equations", Lecture series on Computational Fluid Dynamics, VKI-LS-1982-04, Von Karman Institute for Fluid Dynamics.

Belardini E., Adami P., Martelli F. **"***Development of an Unsteady Parallel Approach for 3D Stator-Rotor Interaction"* 4th European Conference on Turbomachinery, Fluid Dynamics and Thermodynamics- Firenze 20-23 March 2001, Accepted for publication on ImechI Journal of Power and Energy

Centaur™ by CentaurSoft, www.centaursoft.com

Cho, N.-H., Liu, X., Rodi, W., Shönung, B., 1993, "Calculation of Wake-Induced Unsteady Flow in a Turbine Cascade", ASME Journal of Turbomachinery, October, Vol.115, pp. 675-686.

Connel, S.D. and Braaten, M.E., 1995, "Semistructured Mesh Generation for Three-Dimensional Navier-Stokes Calculations" AIAA J., Vol. 33, No. 6, June.

Dawes, W.N., 1992, "The Simulation of Three-Dimensional Viscous Flow in Turbomachinery Geometries Using a Solution-Adaptive Unstructured Mesh Methodology" Transaction of ASME Vol. 114, July.

Delanaye, M., Essers, J.A., 1997, "Finite Volume Scheme with Quadratic Reconstruction on Unstructured Adaptive Meshes Applied to Turbomachinery Flows", J. of Turbomachinery, Vol. 119.

Dénos R., Sieverding C.H., Arts T., Brouckaert J.F. and Paniagua G., 1999, "Experimental Investigation of the Unsteady Rotor Aerodynamics of a Transonic Turbine Stage", 3rd European Conference on Turbomachinery. London.

Durbin, P.A., "On the k-e Stagnation Point Anomaly", Int. J. Heat and Fluid Flow, 1996, 17, 89-90.

Giles, M.B., "Stator-Rotor Interaction in a Transonic Turbine", AIAA-88-3093.

Giles, M.B., 1988, "Stator-Rotor Interaction in a Transonic Turbine", AIAA-88-3093.

Haselbacher, A., McGuirk, J.J., Page, G.J., 1999, "Finite Volume Discretization Aspects for Viscous Flows on Mixed Unstructured Grids" AIAA J., Vol. 37, No. 2.

Hazarika, B.K., Hirsch, C., (1995), "Transition over C4 leading edge and measurements of intermittency factor using pdf of hot-wire signal", ASME 95-GT-294.

Ho, Y.-H., Lakshminarayana, B., "Computation of Three-Dimensional Steady and Unsteady Flow Through a Compressor Stage", ASME 96-GT-070.

Hoogendoorn, C.J., de Lange, H.C., van Steenhoven, A.A., van Dongen, M.E.H., 1997, "Influence of Turbulence Intensity on Intermittency Model in By-Pass Transition", ASME 97-GT-473.

Jameson, A., "Time Dependent Calculations Using a Multigrid with Applications to Unsteady Flows Past Airfoils and Wings", AIAA Paper 91-1596.

Jameson, A., 1991, "Time Dependent Calculations Using a Multigrid with Applications to Unsteady Flows Past Airfoils and Wings", AIAA Paper 91-1596.

Jameson, A., Schmidt, W., Turkel, E., 1981 : "Numerical Solutions of the Euler Equations by Finite Volume Methods Using Runge-Kutta Time-Stepping Schemes", AIAA 81-1259.

Johnson, M.W., Ercan, A.H., 1997, "Predicting Bypass Transition: A Physical Model Versus Empirical Correlations", ASME 97-GT-475.

Jourden, J., Channez, 1992, "Navier-Stokes Flow Simulation in a 2D High Pressure Turbine Cascade with a Cooled Slot Trailing Edge", Proceedings "Recent Advances in Compressor and Turbine Aerothermodynamics", Maison de la Mecanique, Courbevoie, France, 24-25 November.

Kwon, O.J. and Hah, C., 1995, "Simulation of Three-Dimensional Turbulent Flows on Unstructured Meshes" AIAA J. Vol.33, No. 6, June.

Martelli, F., Michelassi, V., Boretti, A.A., 1992, "Numerical Modelling of Coolant Jet Flow in Turbine Cascades", Revue Francaise de Mecanique, No. 4.

Mayle, R.E., "The Role of Laminar-Turbulent Transition in Gas Turbine Engines", ASME Journal of Turbomachinery, 1991, vol. 113, October, pp. 509-537.

Michelassi, V., Adami, P., Martelli, F., (1996), "An Implicit Algorithm for Stator-Rotor Interaction Analysis", IGTI Conference, Birmingham, UK, June 10-13.

Michelassi, V., Martelli, F., 1993, "3-D Implicit Navier-Stokes Solver for Internal Turbulent Compressible Flows", Journal de Phys. III, France 3, pp. 223-235.

Michelassi, V., Martelli, F., Denos, R., Arts, T., Sieverding, C.H., “Unsteady Heat Transfer in Stator-Rotor Interaction by Two Equation Turbulence Model”, International Gas Turbine Conference , Stockholm, Sweden, Accepted for publication in the ASME Journal of Turbomachinery, 1998.

Michelassi, V., Rodi, W., Giess, P.-A., “Experimental and Numerical Investigation of Boundary-Layer and Wake Development in a Transonic Turbine Cascade”. Aerospace Science and Technology Journal, 1998, no.3 191-204 (also IGTI Conference, 1997 Orlando, Florida).

Moss, R.W., Ainsworth, R.W., Sheldrake, C.D., Miller, R., “The Unsteady Pressure Field over a Turbine Blade Surface: Visualisation and Interpretation of Experimental Data”, ASME 97-GT-474.

Pulliam,T.H., Chaussee, D.S., 1981, "A Diagonal Form of an Implicit Approximate-Factorisation Algorithm". Journal of Computational Physics, N. 39.

Rao, K, Delaney, R.A., Dunn, “Vane-Blade interaction in a Transonic Turbine, Part II - Heat Transfer”, AIAA 92-3324.

Rao, K., and Delaney, R. A., "Investigation of Unsteady Flow Through a Transonic Turbine Stage, Part I, Analysis", AIAA Paper 90-2408.

Roe P.L., 1986 “Characteristic based scheme for Euler equations” , Ann. Rev. Fluid Mech., 18.

Saad, Y., 1994 "Krylov Subspace Thechniques, Coniugate Gradients, Preconditioning and Sparse Matrix Solvers", CFD VKI LS 1994-05 VonKarman Institute for Fluid Dynamics.

Saad, Y., 1994, "Krylov Subspace Techniques, Coniugate Gradients, Preconditioning and Sparse Matrix Solvers", CFD VKI LS 1994-05 VonKarman Institute for Fluid Dynamics.

Sieverding C.H., Dénos R., Arts t., Brouckaert J.F., Paniagua G., “Experimental Investigation of the Unsteady Rotor Aerodynamics and Heat Transfer of a Transonic Turbine Stage, VKI Lecture Series on "Blade Row Interference Effects in Axial Turbomachinery Stages", February 1998,

Sieverding, C.H., Heinemann, H., “The influence of Boundary Layer State on Vortex Shedding from Flat Plates and Turbine Cascades”, 89-GT-296, 1989.

Simon F.F., and Stephens, C.A., 1991 “Heat transfer in Bypass Transitional B-L Flows” NASA Tech. Paper 3170

Steelant, J. And Dick, E., 1999, “Calculation of Transition in turbine Cascades by Conditioned N-S Equations”, Third European Conference on Turbomachinery, London

Suzen Y.B., Huang, P.G., 2000, “An Intermittency Transport Equation for Modelling Flow Transition” 38th Aerospace Sciences Meeting & Exhibit, RENO, NV.

Vicedo, J., Vilmin, S., Dawes, W.N., Savill, A.M., 2000, “Extension of Intermittency Transport Modelling to Natural Transition in Internal Aerodynamic Applications”, Proc. Royal Aeronautical Society – Aerodynamics Research Conference, London April.

Wilcox, D.C., "Reassessment of the Scale-Determining Equation for Advanced Turbulence Models", AIAA Journal, 1988, Vol. 26, No.11, pp. 1299-1310.

Acknowledgement The authors want to thanks Prof. V. Michelassi for his support and suggestions in developing the work and acknowledge gratefully the European Commission (TATEF Project) and ASI for supporting the research.

Paper Number: 33

Name of Discusser: H. B.Weyer, DLR Cologne

Question:
Which are the differences in heat transfer coefficients using unstructured and hybrid structured grids?

Answer:
The two codes provide the same early transition start. But after they exibit a difference in the first part of the turbulent boundary layer maybe because of big difference in grids and in the value of y^+ of the first point. It is about 0.5 for unstructured and > 2.0 for structure one.

Name of Discusser: K. Patel, PWC Canada

Question:
You showed mismatch between experimental and numerical method in Mn in the front 20 % of such on side of the blade.
This mismatch is caused by from your presentation, angel of attack difference. Did you try to match this date by changing boundary conditions and if so, did the rest of the aerofoil match experimental and numerical results?

Answer:
We tried to change the rotation speed of the rotor and got better results...

This page has been deliberately left blank

Page intentionnellement blanche